

Dynamic modelling of ORC system for vessel waste heat recovery

**Georgios Verykokkos^a, Efstratios Varvagiannis^b, Konstantinos Braimakis^c
and Sotirios Karellas^d**

^a National Technical University of Athens, Athens, Greece, george_verykokkos@mail.ntua.gr

^b National Technical University of Athens, Athens, Greece, svavv@mail.ntua.gr

^c National Technical University of Athens, Athens, Greece, mpraim@central.ntua.gr

^d National Technical University of Athens, Athens, Greece, sotokar@mail.ntua.gr

Abstract:

The present study presents the dynamic modelling in Dymola software of a vessel waste heat recovery Organic Rankine Cycle-ORC operating with R1233zd(E) that functions as a topping cycle of a cascade prototype also involving an Ejector Vapor Compression Cycle-EVCC as a bottoming cycle developed in the framework of the ZHENIT project. The ORC is designed to have a nominal thermal input of about 95 kW_{th} and is driven by Therminol VP1 oil at inlet and outlet temperatures of 150 °C and 130 °C while it includes two operating modes: 1) electricity-only, in which a recuperator is used and the condensation temperature is low and 2) combined heat and power (CHP), in which the recuperator is bypassed and the condensation temperature is raised to produce hot water. At the system design point, the evaporation temperature is 120 °C, the condensation temperature 30°C and 50°C for electricity-only mode and CHP mode respectively, the superheating degree at expander inlet 10 K and the subcooling degree at condenser outlet 5 K. The system dynamic behavior is investigated considering a pump and expander reduction speed from 100% to 80% of the nominal. According to the results, the system has a fast response to the aforementioned disturbances.

Keywords:

Combined heat and power; Dynamic modelling; ECOS Conference; Electricity production; Organic Rankine cycle; Waste heat recovery.

1. Introduction

1.1. Basics of dynamic modelling

Organic Rankine Cycle (ORC) plays an important role in decarbonisation, especially in the field of waste heat recovery (WHR) in shipping, due to its effectiveness for the conversion of medium and high temperature waste heat into power [1]. ORC is an attractive WHR technology owing to its high reliability and simple design [2]. Because vessel engines operate extensively under variable loads, their waste heat has an intensely fluctuating profile (temperatures, flow rates), which poses technical challenges in the design and operation of ORC systems [3-4]. Therefore, dynamic modelling of ORC systems is necessary to predict their behavior and implement the essential control strategies for effective waste heat utilization, since dynamic models are able to trace the variation of the system operating parameters and detect critical points and outranges. In general, the dynamic behavior of a system including mechanical, electrical, fluid, thermal etc., can be described by a set of transient differential equations (ODE or PDE). The basic concepts that have to be known in dynamic modelling include system inertia, initial conditions, input stimulus variable and time constant [5].

1.2. Organic Rankine Cycles' dynamic operation

Dynamic behavior of ORCs is of interest during their start-up and shut-down and while their operating conditions are varied to respond to fluctuating boundary conditions (heat source, heat sink) to ensure their safe and efficient operation. The main investigated factors include [6]:

- the total system response time, overshoots, and identification of limitations and outranges
- recognition of the start-up and shut-down operation mode
- the part-load capability of the system

A prototype of the ORC system which is presented in this study is going to be developed in the context of the ZHENIT project, focusing on vessel engine WHR at different temperature levels to provide various on-board services. The present work presents the preliminary dynamic modelling of the prototype based on two operating modes: 1) electricity-only 2) Combined heat and power (CHP).

2. Methodology

2.1. System description

The prototype which is going to be developed within the ZHENIT project consists of a cascade ORC (topping cycle) integrated with an ejector-vapor compression cycle (bottoming cycle), utilizing heat sources of temperature levels ranging from 60 °C (jacket cooling water) to 150 °C (engine flue gas) for the production of electricity, heating and cooling. A micro-scale prototype (10 kW_e) will be constructed and demonstrated at lab-scale, along with other alternative proposed WHR solutions.

In the present study, only the topping cycle (ORC) of the aforementioned cascade system is presented, which operates under two modes: electricity-only and CHP mode and is driven by Therminol VP1 oil at a temperature of 150°C. The two modes are simulated through Dymola software [7]. The layout of the system is illustrated in **Figure. 1**.

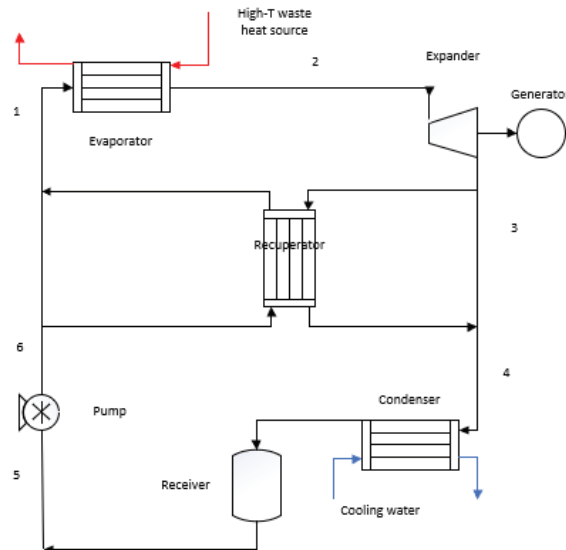


Figure. 1. ORC layout (2 first operating modes)

After a parametric study between three hydrofluoroolefins (HFOs), R1233zd(E) was proven to be the most suitable working fluid, considering its low environmental impact [low global warming potential (GWP) and ozone depletion potential (ODP)], following the regulations of Montreal [8] and Kyoto [9] protocol, as well as the F-gases regulations [10]. What is more, R1233zd(E) has no flammability, according to ASHRAE safety classification and relatively higher critical temperature, leading to higher cycle efficiency. The values of R1233zd(E) properties are mentioned in **Table 1**.

Table 1. R1233zd(E) properties

Working fluid	T _{crit} (°C)	p _{crit} (bar)	ODP	GWP	ASHRAE safety group
R1233zd(E) (ORC)	165.5	35.7	0	1	A1

2.2. System operating parameters and design point

The design point of the system was determined through a steady-state modelling methodology that is not elaborated in the present study. The values of the design point parameters are shown in **Table 2**. **Reference source not found.** In brief, the waste heat stream is Therminol VP1, which enters and exits the evaporator at 150 °C and 130 °C, respectively. The evaporation temperature (T_{evap}) for both modes was considered 120 °C, while the condensation temperature (T_{cond}) is 30 °C in electricity-only mode (Mode 1) and 50 °C in CHP mode (Mode 2).

The net electrical power output of the ORC (P_{el,net}) is defined as the gross electrical output of the expander (P_{el,exp}) minus the electrical power consumed by the pump (P_{el,pump}) and is given by the Eq. (1), considering also the expander-generator electromechanical efficiency (η_{em,exp-G}) and the pump motor efficiency (η_{M,pump}). The numeric subscripts (e.g. 2, 3) correspond to the points of the system layout in **Figure. 1**.

$$P_{el,net} = P_{el,exp} - P_{el,pump} = \dot{m}_{wf} \cdot \left(\eta_{em,exp-G} \cdot (h_2 - h_3) - \frac{(h_6 - h_5)}{\eta_{M,pump}} \right) \quad (1)$$

Table 2. ORC prototype design-point parameters

	Mode 1 (electricity-only)	Mode 2 (CHP)
Heat source mass flow rate (kg/s)		2.5 kg/s
Heat source inlet temperature (°C)		150
Heat source outlet temperature (°C)		130
Expander isentropic efficiency		0.70
ORC pump isentropic efficiency		0.65
Expander-generator electromechanical efficiency		0.92
ORC pump motor efficiency		0.95
Superheating degree at expander inlet (K)		10
Subcooling degree at condenser outlet (K)		5
ORC working fluid		R1233zd(E)
ORC evaporation temperature (°C)		120
ORC condensation temperature (°C)	30	50
Cold stream temp. rise in recuperator (K)	20	-
Electrical power output (kW _e)	11.35	8.06
Heating output (kW _{th})	-	85.5
ORC electrical efficiency (%)	12.84	10.01

The heat input to the cycle ($\dot{Q}_{evap,ORC}$), is calculated according to Eq. (2), where \dot{m}_{wh} , $h_{wh,in}$ and $h_{wh,out}$ are the waste heat stream 's mass flow rate and enthalpies at the inlet and outlet of the evaporator respectively.

$$\dot{Q}_{evap,ORC} = \dot{m}_{wf}(h_2 - h_1) = \dot{m}_{wh}(h_{wh,in} - h_{wh,out}) \quad (2)$$

2.3. ORC dynamic modelling in component level

To develop a robust and concurrently a relatively fast dynamic model it is imperative to choose the proper components, correct initial conditions and to consider appropriate simplifying assumptions for the overall model. For instance, there are various types, sizes and modelling approaches for the heat exchangers, pumps, expanders etc. Consequently, in this point the types and the approaches of the models that were used in the model are described briefly.

2.3.1. Heat exchangers

The system heat exchangers (evaporator, condenser, recuperator) were modelled using the finite volume method, according to the available models that are included in the Thermocycle library [11]. In this method, the flow length of the heat exchanger is discretized into n equal volumes (cells), in which the equations of mass and energy conservation are applied.

The properties of the fluid for each volume can be calculated either at the mean states of the two nodes ("central scheme"), or it can be assumed that the properties of the fluid for each volume are equal to the properties of the fluid leaving the volume ("upwind scheme"). If the fluid flows only in one direction, the upwind scheme is more robust. The central scheme is more computationally intensive than the upwind scheme, but it deals better with discontinuities in the case of flow reversal. For the heat exchangers of the present study the upwind scheme was implemented. The properties of the fluid at the cell boundaries are represented by the symbol "*" in **Figure. 2**. The area of cell, volume of cell, temperature and enthalpy at each node are given by the following equations [Eq. (3), Eq. (4)] [12]:

$$A_i = \frac{A}{n}; \quad V_i = \frac{V}{n}; \quad i = 1,2,3, \dots, n \quad (3)$$

$$T_i = \frac{T_{i+1}^* + T_i^*}{2}; \quad h_i = \frac{h_{i+1}^* + h_i^*}{2}; \quad i = 1,2,3, \dots, n \quad (4)$$

The mass balance and the energy balance for each side and cell of the heat exchanger are given by Eq. (5) and Eq. (6) respectively:

$$\frac{dm_i}{dt} = \dot{m}_i^* - \dot{m}_{i-1}^* \quad (5)$$

$$\frac{dU_i}{dt} = (\dot{m}_{i-1}^* h_{i-1}^* - \dot{m}_i^* h_i^*) + \dot{Q}_i \quad (6)$$

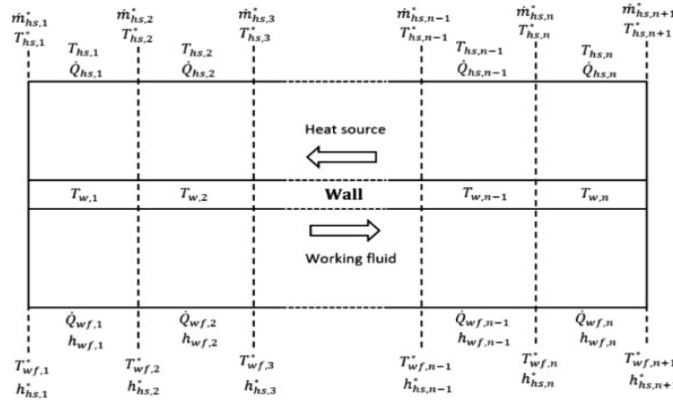


Figure 2. Finite volume modelling approach of the heat exchangers [13]

Furthermore, for the modelling of the heat exchangers the following assumptions are considered:

- One-dimension fluid flow in the heat exchangers
- Constant heat flow per area unit and linear allocation of specific enthalpy in every control volume
- Negligible gravity forces in the fluid flow
- Negligible pressure drops in the heat exchangers and the pipes

2.3.2. Expander

For the dynamic modelling of the system a volumetric screw expander is used. The dynamics of the expander and the pump are very fast compared to those of the heat exchangers and are modelled at steady-state. Neglecting the heat loss, a volumetric expander can be modelled by its isentropic efficiency and filling factor, given by Eq. (7) and Eq. (8) respectively:

$$\eta_{exp,is} = \frac{W_{exp}}{\dot{m}_{wf}(h_{exp,in} - h_{exp,out,is})} \quad (7)$$

$$ff = \frac{\dot{m}_{wf}}{\rho_{exp,in} V_{sw} N_{exp}} \quad (8)$$

The work output of the expander is given by Eq. (9):

$$\dot{W}_{exp} = \dot{m}_{wf}(h_{exp,in} - h_{exp,out}) \quad (9)$$

Expander boundary conditions are pressure and enthalpy at the inlet and pressure at outlet. In addition, the inlet and outlet are considered adiabatic.

Through the work of the expander, the net electrical power output and the waste heat energy as defined in Eq. (1) and Eq. (2) respectively, the ORC electrical efficiency is calculated and given by Eq. (10):

$$\eta_{el,ORC} = \frac{P_{el,net}}{Q_{evap,ORC}} \quad (10)$$

2.3.3. Pump

Similarly, the dynamic response of the working fluid pump is very fast compared to that of the system heat exchangers. Hence, the pump is modelled by a steady-state lumped parameter model. In the present dynamic system, a centrifugal pump is used, whose role is to maintain the pressure and the mass flowrate of the working fluid. Usually for this type of pump the volume flow rate is a function of both the head and the rotational speed. However, in this model there is also the ability to define the mass flow as an input parameter. As a result, the pump power consumption and outlet temperature are calculated by the following equations [Eq. (11), Eq. (12)]:

$$P_{pump} = \frac{\dot{m}_{pump}(p_{out,pump} - p_{in,pump})}{\rho \eta_{is,pump}} \quad (11)$$

$$T_{out,pump} = T_{in,pump} + \frac{(1 - \eta_{is,pump}) P_{pump}}{\dot{m}_{pump} c_{pump}} \quad (12)$$

2.3.4. Tank

A tank in an ORC system operates as a buffer storage for the working fluid to provide fluid or accumulate it during the transition phase of the system (start-up, part-load operation or shut-down). To calculate the working

fluid properties, the mass balance [Eq. (13)] and energy balance [Eq. (14)] are applied in the tank, while the tank level is calculated by Eq. (15), where V_0 is the initial total fluid volume in the tank.

$$\frac{dm_f}{dt} = \dot{m}_{f,in} - \dot{m}_{f,out} \quad (13)$$

$$\frac{d(E)}{dt} = \dot{m}_{in}h_{in} - \dot{m}_{out}h_{out} \quad (14)$$

$$H_{tank} = \frac{V}{V_0} \quad (15)$$

2.4. ORC system modelling

Based on the modelling of each individual component, the overall ORC system was modelled in Dymola through the Modelica language [14], as indicated in **Figure. 4** for Mode 1 and in **Figure. 3** for Mode 2.

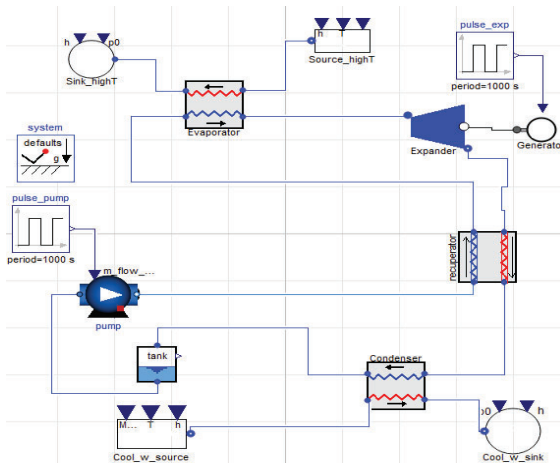


Figure. 4. Dymola ORC system layout (mode1)

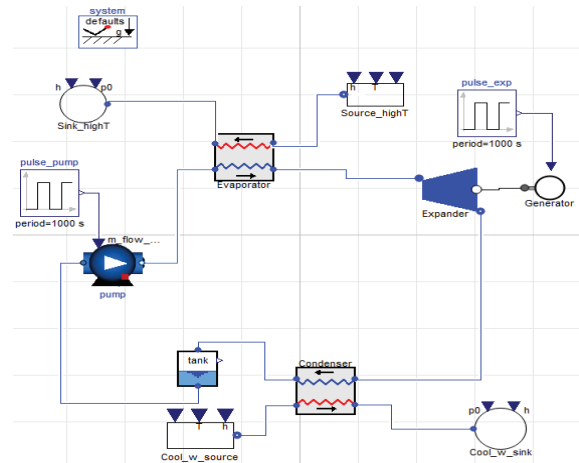


Figure. 3. Dymola ORC system layout (mode2)

During the modelling, the pressure drops of the pipes are omitted. Additionally, the system begins in steady-state (to avoid any discontinuities and consequent errors during the start-up) using initial conditions and then comes to a new steady-state after internal disturbances have been applied (heat transfer, mass flow etc). After that, a specific disturbance is imposed and the system results in a new steady-state. Two different scenarios regarding the type of the implemented disturbance are investigated, with alteration of the mass flow rate of the pump and change of the rotational speed of the expander. When the imposed disturbance ceases, the system returns to the initial steady-state. After a relevant investigation, it was inferred that a time period of 1000 s is well enough for the system to establish the steady-state. Thus, 1000 s is the time period that each disturbance lasts during the simulations.

3. Results and discussion

3.1. Initial conditions for the system

As mentioned before, the initial conditions of the system are selected so that the system reaches initially the steady-state at the design point. The two following scenarios are investigated for each mode:

Scenario 1: part-load operation of the system, reducing the pump mass flow rate at the 80 % of the nominal point and then bringing it back to the initial value

Scenario 2: part-load operation of the system, reducing the rotational speed of the expander at the 80 % of the nominal point and then bringing it back to the initial value

The initial conditions that have been defined for the system, after a relevant parametric analysis are presented in the **Table 3**.

For the simulations of Scenario 1 for both modes the pump mass flow rate is 0.435 kg/s for the first 1000 s, then it is reduced at 0.385 kg/s for the next 1000 s and finally it increases again at its initial value for the last 1000 s.

Likewise, for the simulations of Scenario 2 for both modes the rotational speed of the expander is 2400 rpm for the first 1000 s, then it is reduced at 1950 rpm for the next 1000 s and eventually it increases again at its initial value for the last 1000 s.

Table 3. Initial input conditions of the system

	Mode 1 (electricity-only)	Mode 2 (CHP)
Heat source mass flow rate (kg/s)		2.5
Heat source inlet temperature (°C)		150
Heat source outlet temperature (°C)		130
Nominal working fluid mass flow rate (kg/s)		0.435
Working fluid outlet temperature from the evaporator (°C)		130
Working fluid outlet temperature from the condenser (°C)	25	45
Recuperator cold stream temperature rise (K)	20	-
Cooling water mass flow rate (kg/s)	3.94	3.94
Cooling water temperature inlet in condenser (°C)	15	25

Each simulation run is conducted for 3000 s with a time step of 6 s for each iteration and a tolerance of 0.0001 for the convergence of each iteration. Also, a noticeable feature is that it needs almost 170 s and 63 s in real time for the systems of Mode 1 and Mode 2 respectively to converge during the simulation.

3.2. Mode 1 results

To begin with, an important characteristic of the system is the temperature of the working fluid at the evaporator outlet, as, along with the pressure, it can be used for determining the superheating degree. The variation of this parameter for the scenarios of Mode 1 is depicted in **Figure. 5**. As it is illustrated in this diagram, initially the evaporator outlet temperature is 130 °C for both scenarios, corresponding to the design parameter (120 °C and 10 °C superheating). During the disturbance, in the first scenario the examined temperature is increased, because, although the heat recovered from the heat source remains approximately the same [slightly lower due to reduction of the evaporator heat transfer coefficient (U)], the working fluid mass flow rate decreases and thus more energy is absorbed per working fluid unit mass. Furthermore, the fluctuation of the working fluid pressure in the evaporator is shown in **Figure. 6**. At the design point, the evaporator pressure is 15.7 bar, equal to the design evaporation pressure. On the contrary, when the disturbance occurs, in Scenario 1 the evaporator pressure decreases, as less working fluid mass passes through the expander, which has the same rotational speed. Thus, less pressure is required at the inlet of the expander in order for the working fluid to enter the expander. In the second scenario, in which the rotational speed of the expander is decreased, the evaporator outlet temperature is reduced. Inside the evaporator there is a constant volume of working fluid and while its density rises due to the pressure increase, there is more working fluid mass accumulated in the evaporator. The accumulated working fluid absorbs more thermal energy resulting in the reduction of the evaporator outlet temperature. Regarding the pressure, in Scenario 2 it increases, since the lower speed of the expander does not facilitate the passage of the working fluid, whose mass flow rate is imposed by the pump and remains constant. Hence, it needs to increase the pressure difference in the expander through higher pressure at its inlet. Furthermore, it is remarkable that in Scenario 2, although the pressure and subsequently the evaporation temperature rise, there is some liquid formed at the evaporator outlet reducing the temperature of the working fluid at the vapor saturation temperature (there is no superheating).

It is notable that the hypothesis of constant heat flow along the heat exchanger, which is implemented during the modelling of the heat exchangers, is validated by the fact that the inlet and outlet temperatures of the heat source are 150 and 130 °C, while the evaporation temperature is 120 °C. Thus, at the evaporator inlet and outlet there is an alteration of the temperature difference of the same order of magnitude. The impact of this hypothesis on the results is the easier convergence of the total system and the smooth temperature increase along the heat exchanger. What is more, as it is also shown in the following figure, the system response during the implemented disturbances is rapid, as the system reaches a new steady state quite fast.

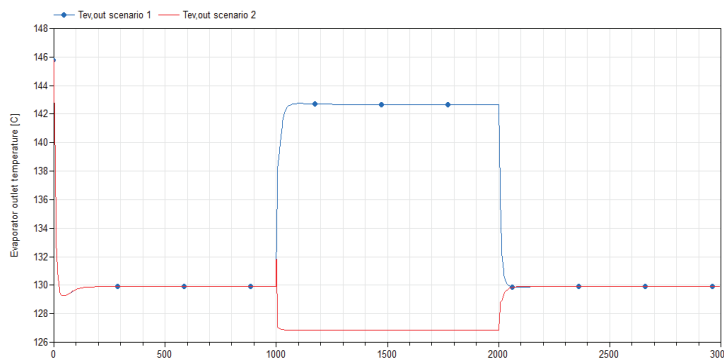


Figure. 5. Evaporator outlet R1233zd(E) temperature for scenarios 1 & 2 (Mode 1)

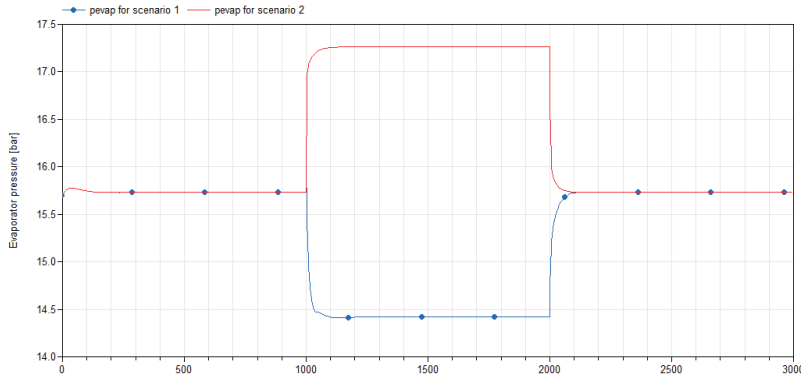


Figure 6. Evaporator working fluid pressure for Mode 1

In **Figure 7**, the inlet and outlet temperatures of the cold stream of the recuperator are shown. At the design point the temperature rise of the cold stream is indeed 20 K equal to the design parameter, while during the imposed disturbance, the system reaches fast to a new steady state. In Scenario 1 the cold stream temperature rise in the recuperator increases, while in Scenario 2 the respective value decreases. The heat transfer in the recuperator is described by Eq. (16):

$$\dot{Q} = \dot{m}_{wf} c_p \Delta T \quad (16)$$

As a result, when the mass flow rate of the working fluid declines in Scenario 1 and the temperature of the fluid at the expander inlet rises, the thermal heat rate is increased. In this way, the temperature difference of the cold stream is increased so as to counterbalance the reduction of the mass flow rate. On the contrary, in Scenario 2, in which the rotational speed of the expander and its inlet temperature decline, the outlet temperature of the expander is also reduced, resulting in lower heat rate transferred to the cold stream. Thus, because the mass flow rate remains constant, the cold stream temperature difference decreases.

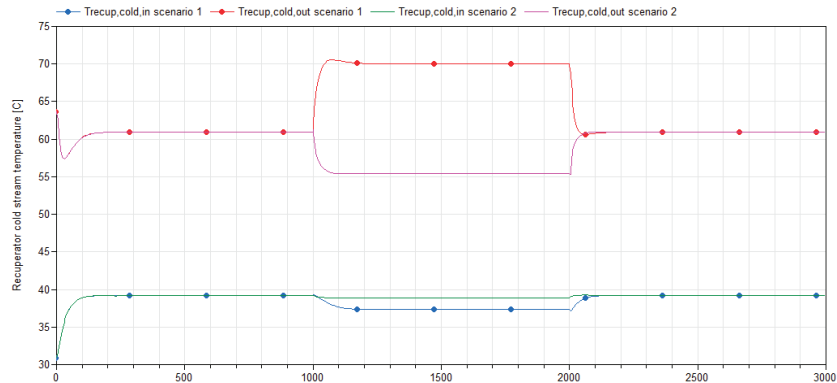


Figure 7. Recuperator cold stream temperatures for scenarios 1 & 2 of Mode 1

The following diagrams demonstrate the working fluid temperature at the condenser outlet (**Figure 8**) and the condenser pressure (**Figure 9**) for the system of Mode 1 and the scenarios 1 and 2 respectively. As it is illustrated in the relevant diagram, during the dynamic modelling the working fluid temperature at the condenser outlet and at the design point, as well as the condensation temperature, is approximately 37 °C, namely 7 °C higher than the respective design point value. Similarly, the condenser pressure at the design point is 1.96 bar, higher than the design point condensation pressure. These significant differences are justified by the high complexity of the overall system and the fact that the design parameters of the heat exchangers, the expander and the pump have not been taken into account in the thermodynamic design of the system. In Scenario 1, the condenser outlet temperature of the working fluid and its pressure are reduced. This is due to the fact that the working fluid mass flow rate is decreased, while the cooling water mass flow rate and inlet temperature remain constant. Consequently, the working fluid is cooled in higher degree (lower outlet temperature and condenser pressure). In Scenario 2, the condenser outlet temperature and pressure remain stable, since the mass flow rate of the working fluid does not change and only the recuperator is affected by the reduced temperature at the expander outlet.

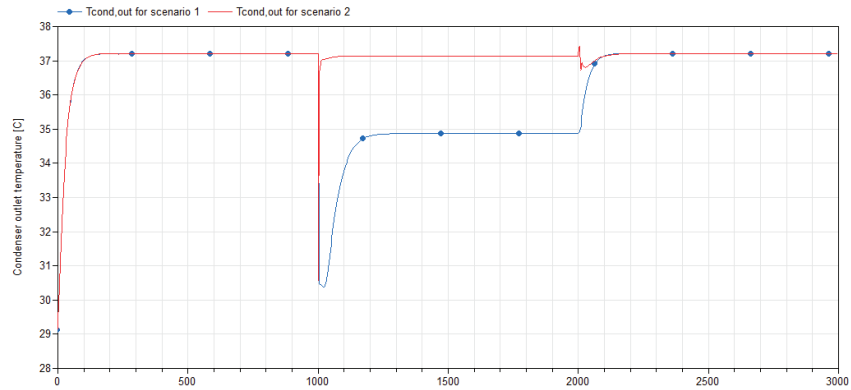


Figure 8. Condenser outlet R1233zd(E) temperature for scenarios 1 & 2 (Mode 1)

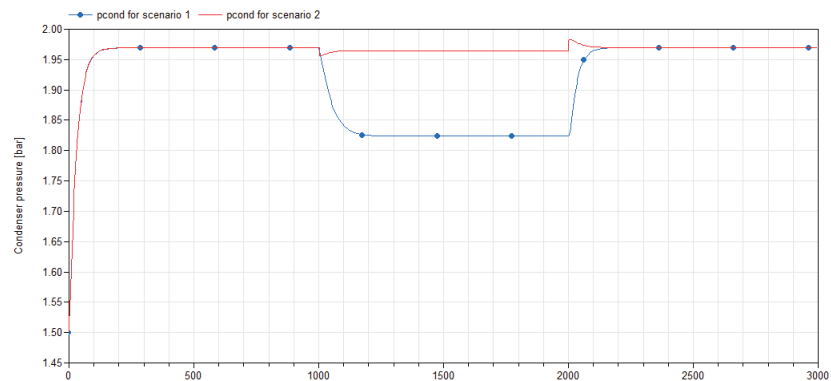


Figure 9. Condenser working fluid pressure for Mode 1

As it is described in **Figure 10**, the net electrical power output of the system for both scenarios at the design point is approximately 11280 W, almost equal as the design parameter of 11.35 kW (0.6 % lower). When the disturbance is imposed, in both scenarios the electrical power output is reduced because of the reduction of the working fluid mass flow rate (and lower expander inlet pressure and pressure difference as indicated before) and the rotational speed of the expander (lower evaporator outlet temperature and no superheating at expander inlet) respectively.

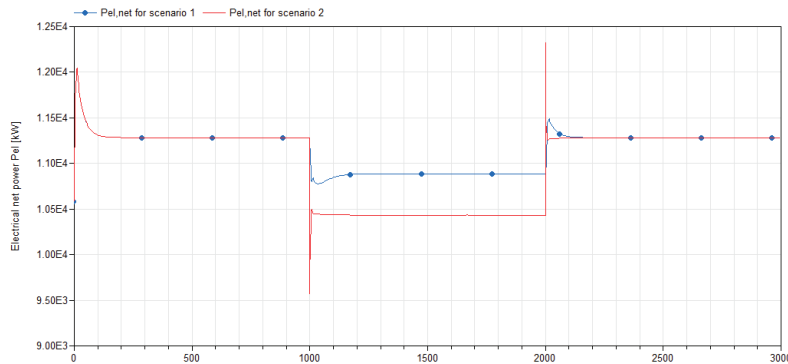


Figure 10. System electrical net power (Mode 1)

It is worth pointing out that the heat source transfers 92.66 kW to the evaporator of the system at the design point. Therefore, the electrical efficiency of the system at the design point, according to Eq. (1), is 12.17 %, declining in 11.87 % and 11.40 %, due to the net electrical power output reduction, as long as the external disturbance lasts in Scenario 1 and 2 respectively. Moreover, as it is demonstrated from the diagrams of the system parameters for Mode 1, the system needs approximately 300 s in simulation time, to reach a new steady-state after an alteration in its parameters.

3.3. Mode 2 results

The temperature of the working fluid at the evaporator outlet for both scenarios of Mode 2 is demonstrated in **Figure. 11**, while the evaporator pressure for the correspondent cases is illustrated in **Figure. 12**. During the imposed disturbance, in the first scenario the examined temperature is increased, whereas in the second scenario the outlet temperature from the evaporator declines, following the trend of Mode 1 for similar reasons. At the design point the pressure is almost 15.7 bar, equal to the evaporation pressure. At the Scenario 1, the pressure of R1233zd(E) is reduced, as well as its mass flow rate, while lower expander rotational speed leads to the increase of the evaporator pressure in Scenario 2, for the same causes as in Mode 1.

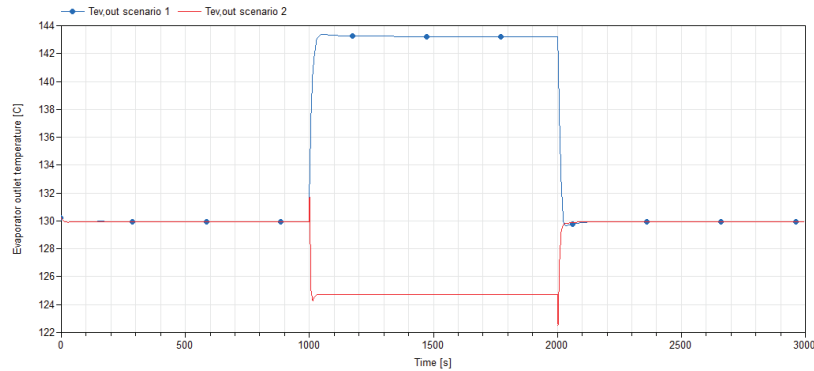


Figure. 11. Evaporator outlet R1233zd(E) temperature for scenarios 1 & 2 (Mode 2)

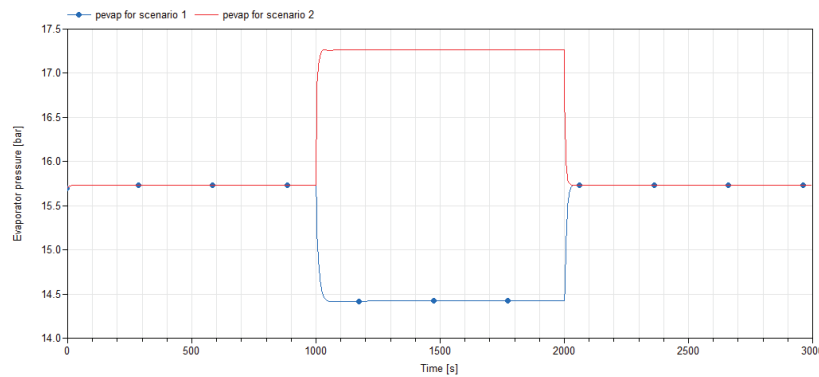


Figure. 12. Evaporator working fluid pressure for Mode 2

Moving to the condenser analysis, at the design point the working fluid outlet temperature (**Figure. 13**) is slightly lower than 50 °C, which is the condensation temperature. In other words, R1233zd(E) exits the condenser lightly subcooled, being close to the saturation curve, but in the one-phase region along the whole simulation. During the disturbance, in Scenario 1 the temperature of the fluid after the condenser is lower for the same reason as it happens in the evaporator, while in Scenario 2, due to lower expander speed, the temperature at the expander outlet is lower, as mentioned above. Hence, because the cooling water parameters remain unchanged, the working fluid is cooled in a higher degree.

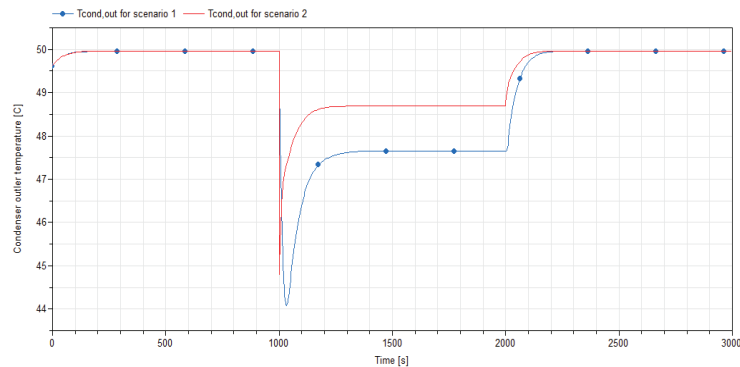


Figure. 13. Condenser outlet R1233zd(E) temperature for scenarios 1 & 2 (Mode 2)

Figure. 14 illustrates the condenser working fluid pressure, whose value at the design point is 2.93 bar just like the design parameter. During the disturbance, the pressure declines similarly to the working fluid temperature at the outlet of the condenser.

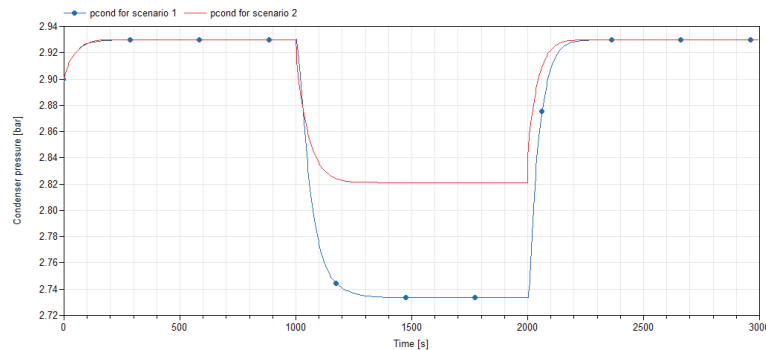


Figure. 14. Condenser working fluid pressure for Mode 2

Afterwards, in **Figure. 15** the net electrical power output of the system is demonstrated. At the design point, the electrical net power is almost 7800 W, approximately 2.5 % lower than its design value. This deviation is owed to the fact that the design parameters of the system components have not been taken into account in the thermodynamic design, as well as because of the fact that R1233zd(E) was inserted in Dymola via CoolProp [15], which also contain some slight errors regarding its thermodynamic properties. In scenarios 1 and 2, the net power is reduced due to similar causes as in Mode 1.

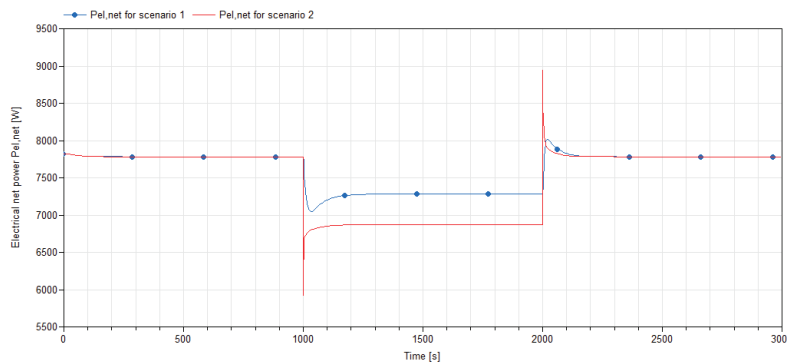


Figure. 15. System electrical net power (Mode 2)

It is notable that the heating output of the system of Mode 2 at the design point is 92.6 kW (higher than the design point value) decreasing in 89.44 kW and 87.03 kW in Scenario 1 and 2 respectively, while the heat source transfers 99.81 kW to the evaporator of the system at the design point. Therefore, the electrical efficiency of the system at the design point is 7.8 %, declining in 7.6 % and 7.4 % during the external disturbance in Scenario 1 and 2 respectively. The electrical efficiency arising from the dynamic modelling is lower than the design point's one. The difference is owed to the same reasons as the deviation of the net electrical power. These are also the causes of the increased heating output of the system of Mode 2, which contribute to the reduced electrical efficiency.

4. Conclusions

The present study analysed the dynamic modelling of a vessel engine waste heat recovery Organic Rankine Cycle (ORC) system, which makes up the topping of a cascade ORC combined with an ejector vapor-cooling compression cycle (EVCC) and operates in two different modes: 1) electricity-only and 2) combined heat and power (CHP) via heat recovery by the ORC condenser. In the beginning, the basic concepts of dynamic modelling were mentioned briefly and the ORC system was described, as well as its main features and design point operating parameters. Furthermore, the modelling elements and methods at system component level were defined, whereas the total ORC system in Dymola and its simulations' characteristics were highlighted. Eventually, after the presentation of the simulation results for the two modes and two different scenarios [1] reducing the pump mass flow rate at 80% of the nominal one and 2) decreasing the expander rotational speed at the 80% of the nominal one], it was demonstrated that the system, regarding most of its parameters' values, during its steady-state at the design point parameters matches the values of the off design, resulting in net electrical power output up to 11.28 kW (Mode 1) with electrical efficiency of up to 12.17 % (Mode 1). What is

more, the system's response to the disturbances ranges from 250 up to 300 s, whereas some slight deviations from the design point are owed to the fact that the design parameters of the system components have not been considered in its thermodynamic design.

Acknowledgment

This study has been performed within the context of the ZHENIT project, funded by the European Union's Horizon Europe research and innovation program, under grant agreement No. 101056801

Nomenclature

Abbreviations

<i>WHR</i>	Waste heat recovery
<i>ORC</i>	Organic Rankine cycle
<i>LTES</i>	Latent thermal energy storage
<i>ODE</i>	Ordinary differential equations
<i>PDE</i>	Partial differential equations
<i>CHP</i>	Combined heat and power
<i>HFO</i>	Hydrofluoroolefin
<i>GWP</i>	Global warming potential
<i>ODP</i>	Ozone depletion potential
<i>FMI</i>	Functional mock-up interface
<i>EVCC</i>	Ejector vapor cooling cycle

Symbols:

T	temperature, °C
p	pressure, bar
T_H	high temperature
n	number
A	area, m ²
V	volume, m ³
h	enthalpy, J/kg
\dot{m}	mass flow rate, kg/s
\dot{Q}	heat transfer rate, W
U_i	internal energy, J
\dot{W}	work, W
ff	filling factor
N	rotational speed, rpm
P	power, W
C	specific heat capacity, J/(kgK)
U	heat transfer coefficient, W/(m ² K)

Greek symbols

η	efficiency
ρ	density, kg/m ³
ΔT	temperature difference

Subscripts and superscripts

<i>crit</i>	critical
<i>evap</i>	evaporation
<i>cond</i>	condensation
<i>wf</i>	working fluid
<i>em</i>	electromechanical
<i>el</i>	electrical

<i>exp</i>	expander
<i>pump</i>	pump
<i>M</i>	motor
<i>wh</i>	waste heat
<i>in</i>	inlet
<i>out</i>	outlet
<i>i</i>	index
<i>hs</i>	heat source
<i>w</i>	water
<i>sw</i>	swept volume
<i>is</i>	isentropic
0	initial value
<i>ev</i>	evaporator
<i>cond</i>	condenser

References

- [1] Zhai H., An Q., Shi L., Lemort V., Quoilin S., Categorization and analysis of heat sources for organic Rankine cycle systems. *Renewable and Sustainable Energy Reviews* 2016; 64: pp. 790-805
- [2] Li Z., Yu X., Lei W., Jiang R., Yu X., Huang R., Wu J., Comparative investigations of basic ORC and cascaded LTES-ORC under transient heat sources. *Applied Thermal Engineering* 2022; 207
- [3] Li Z., Lu Y., Huang R., Chang J., Yu X., Jiang R., Yu X., Roskilly A.P., Applications and technological challenges for heat recovery, storage and utilisation with latent thermal energy storage. *Applied Energy* 2021; 283
- [4] Da Lio L., Manente G., Lazzaretto A., A mean-line model to predict the design efficiency of radial inflow turbines in organic Rankine cycle (ORC) systems. *Applied Energy* 2017; 205: pp. 187-209
- [5] Assadi M., Barzi Y. M., *Organic Rankine Cycle Technology for Heat Recovery*, 2018, Chapter 6: Dynamic Modeling of ORC Power Plants
- [6] Braden Lee T., *Dynamic simulation and experimental validation of an Organic Rankine Cycle model*, [PhD Thesis, School of Mechanical and Mining Engineering, The University of Queensland], 2016
- [7] Dassault Systemes, Dymola systems engineering, Multi-engineering modelling and simulation based on modelica and FMI – Available at: < <https://www.3ds.com/products-services/catia/products/dymola/> > [accessed 12.3.2023]
- [8] European Parliament, Regulation (EC) No 2037/2000 of the European Parliament and of the Council of 29 June 2000 on substances that deplete the ozone layer. 2000, Council of the European Union
- [9] United Nations, Kyoto Protocol. 1997: Kyoto, Japan
- [10] European Parliament, Regulation (EU) No 517/2017 of the European Parliament and of the Council of 16 April 2014 on fluorinated greenhouse gases and repealing Regulation (EC) No 842/2006. 2014, Council of the European Union.
- [11] Quoilin S., Desideri A., Wronski J., Bell I. H., Thermocycle library – Available at: < <http://thermocycle.squoilin.eu/download/thermocycle-library/> > [accessed 12.3.2023]
- [12] Imran M., Pili R., Usman M., Haglind F., Dynamic modeling and control strategies of organic Rankine cycle systems: Methods and challenges, 2020, *Applied Energy* 276
- [13] Xu B, Rathod D, Kulkarni S, Yebi A, Filipi Z, Onori S, et al., Transient dynamic modeling and validation of an organic Rankine cycle waste heat recovery system for heavy duty diesel engine applications. *Applied Energy* 2017; 205:260–7
- [14] Modelica Association, Modelica language – Available at: < <https://modelica.org/modelicalanguage.html> > [accessed 12.3.2023]
- [15] Bell I. H., Wronski, J., Quoilin S., Lemort V., Pure and Pseudo-pure Fluid Thermophysical Property Evaluation and the Open-Source Thermophysical Property Library CoolProp, *Industrial & Engineering Chemistry Research* 2014,53:2498-2508 – Available at: <<http://www.coolprop.org/>> [accessed 13.3.2023]